Honors Theses   Honors College

Spring 5-2019

Synthesis, Characterization, and Utilization of Iron II Ion Sensing Fluorescent Probes for Detection of Early Onset Anodic Corrosion

Dane N. Wedgeworth
University of Southern Mississippi

Follow this and additional works at: https://aquila.usm.edu/honors_theses

Part of the Polymer Chemistry Commons

The University of Southern Mississippi

Synthesis, Characterization, and Utilization of Iron II Ion Sensing Fluorescent Probes for
Detection of Early Onset Anodic Corrosion

By

Dane Wedgeworth

A Thesis
Submitted to the Honors College of
The University of Southern Mississippi
in Partial Fulfillment
of Honors Requirements

May 2019

Approved by

_____

James W. Rawlins, Ph.D., Thesis Advisor

Professor of Polymer Science

_____

Jeffrey Wiggins, Ph.D., Director

School of Polymer Science and

Engineering

_____

Ellen Weinauer, Ph.D., Dean

Honors College

Abstract

Corrosion effects can be seen in infrastructure all around the world. From rusted bridges, ships, and other steel surfaces, the price of corrosion adds up quickly with repairs, maintenance, and complete replacement. Common approaches to corrosion detection and prevention require slow, optical inspection to begin the repair and maintenance process, which can also be very slow and costly. However, recent literature suggests that metal chelating probes can yield new understanding of the processes of corrosion faster and with greater specificity in location and diversity in mechanisms for early onset of corrosion. Earlier corrosion detection can be characterized by several ways. One method, fluorescence, is a tool used to detect, quantify and observe corrosion. The work provided in this document focuses specifically on a pyrene-TEMPO species that becomes fluorescent by the donation of electrons from metal ions (namely iron II) that are generated at anodic sites in the corrosion process. By observing these events, we will be able to qualitatively detect the early onset of corrosion and potentially quantitatively monitor early corrosion, which would allow for improved timing for maintenance and repairs and less costly repair processes for coated steel substrates. Herein, we report the synthesis, characterization, and utilization of the pyrene-TEMPO species in the solution state, solvated resin state, and final glassy matrix coated state. We report the effect of these three solution and polymer physical states on fluorescence intensity as well as emission wavelengths with and without Fe^{2+}.

Keywords: corrosion detection, metal chelating, fluorescent probes, iron II

Acknowledgements

I would like to express my utmost gratitude to my advisor, Dr. James Rawlins, who has been an amazing mentor and teacher over the past two years of my undergraduate research. He has taught me innumerable life lessons as well as lessons in the research process, and I will be forever grateful for the support he continued to give to me. I would especially like to thank Dr. Dwaine Braasch for his support and countless hours of guidance and patience. I could not have done this project without him. I would like to thank my graduate mentors, Robert Peterson and Jessica Davison, for all their support and counseling with my research as well as my undergraduate career. I would also like to thank the rest of the Thames-Rawlins Research Group for all the help and advice over the past two years.

I would like to thank my parents, Scott and Dana Wedgeworth, for constantly supporting me and my pursuits and raising me to be the person I am today. I would also like to thank my fiancé, Elizabeth Coker, for her countless support and patience over my undergraduate career.

Table of Contents

Contents

List of Figures and Tables

Figures

Tables

List of Abbreviations

Pyr	1-pyrenecarboxyllic acid
DMAP	4-(dimethylamino)pyridine
DCC	Dicyclohexylcarbodiimide
TEMPO	4-hydroxy-2,2,6,6-tetramethylpiperidine
DCM	Dichloromethane
CHCl$_3$	chloroform
ACN	acetonitrile
MEK	methyl ethyl ketone
EEP	3-ethoxypropionate
DCU	Dicyclohexylurea
DCB	Dichlorobenzene
Hex	Hexanes
EtOAc	Ethyl Acetate
NMR	Nuclear Magnetic Resonance
LC/MS	Liquid Chromatography Mass Spectrometry
GC/MS	Gas Chromatography Mass Spectrometry
PT	Pyrene-TEMPO
DGEBA	diglycidilethers of bisphenol A
TLC	Thin Layer Chromatography
ASTM	American Society for the Testing and Materials

1. Introduction and Background

1.1. Corrosion background and mechanism

Corrosion can be defined as the chemical or electrochemical reaction between a substrate, usually a metal, and its environment that produces a deterioration of the substrate and its properties. For example, iron and steel tend to combine with other elements to return to their lowest energy states.[1] The environment includes all materials that have contact with the substrate (i.e. air interface and polymer-substrate interface) such as water, salt, and harmful solvents. There are several common types of corrosion that exist: uniform, galvanic, crevice, pitting, intergranular, erosion, stress, and hydrogen damage. (**Figure I**).[1] The most common type, uniform, involves the chemical or electrochemical attack of the steel, which results in degradation of the material and failure and, therefore, will be the focus of this research.
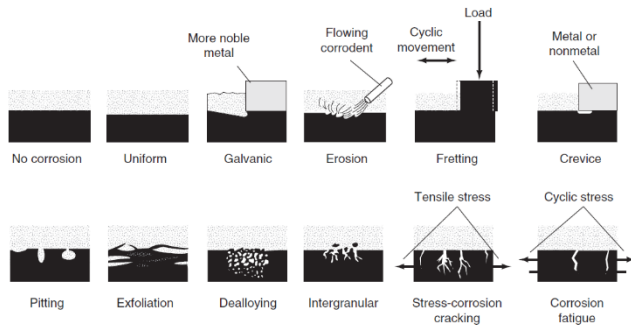
Figure I. Schematics of the common forms of corrosion.[1]
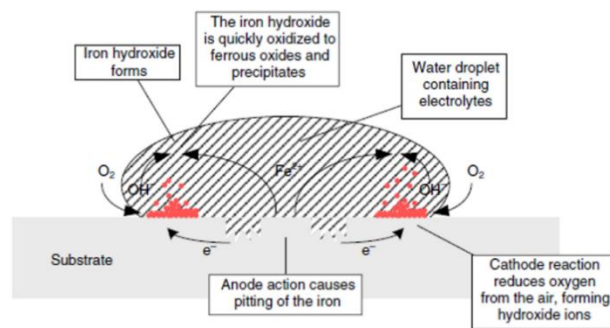
Figure II. Galvanic corrosion process.[3]

Corrosion of a metal substrate requires that water, oxygen or other reducible species, dissolution process at the anode, a cathodic site, and an electrolytic path between the anode and cathode all be present.[2] If one of these is not present, then corrosion can be controlled and limited. The type of corrosion that will be investigated in this research is galvanic (**Figure II**).[3] The diagram depicts the production of iron II ions as well as electrons at the anode. At the

1

cathode, oxygen from the atmosphere is reduced to form hydroxide ions. The hydroxide ions

combine with iron II ions to form iron hydroxide, which is quickly oxidized to ferrous oxides

and precipitates. It is very important to further investigate the specific reactions that occur in the

corrosion process. At the anode, the net reactions yield ferrous ions as well as electrons.[3] This

can be seen in the following reaction: $Fe(s) \rightarrow Fe^{2+}(aq) + 2e^-$. Once combined with hydroxide ions,

the resulting species is oxidized into an unstable green hydrated magnetite: $FeO \cdot Fe_2O_3 \cdot H_2O$.[3]

Since this compound is unstable, it decomposes into black magnetite: $FeO \cdot Fe_2O_3$, and this

compound oxidizes into rust: $Fe_2O_3 \cdot H_2O$.[3] The following reaction scheme depicts the overall

reaction: $6Fe(s) + 4\frac{1}{2}O_2(aq) + 3H_2O(l) \rightarrow 3Fe_2O_3 \cdot H_2O(s)$.[3] This reaction is thermodynamically

driven due to the potential difference between the cathode and anode. So, in order to disrupt the

process, materials must be able to inhibit a large potential difference and possessing effective

barrier methods.

1.2 Anti-Corrosive Coatings Formulations

Three of the most effective ways of controlling corrosion through the use of organic,

polymer coatings are material selection, appropriate polymer binder selection, and

implementation of anti-corrosive pigments. The rate of corrosion is defined as the corrosivity of

environment divided by the corrosion resistance of metal.[1] **Figure III**[3] displays the various

factors that affect the durability of an anti-corrosive coating. So, as the resistance of the metal

increases, rate of corrosion will decrease, and as the corrosivity of the environment increases,

rate of corrosion will increase. Therefore, resistance of the metal is important when selecting

materials.
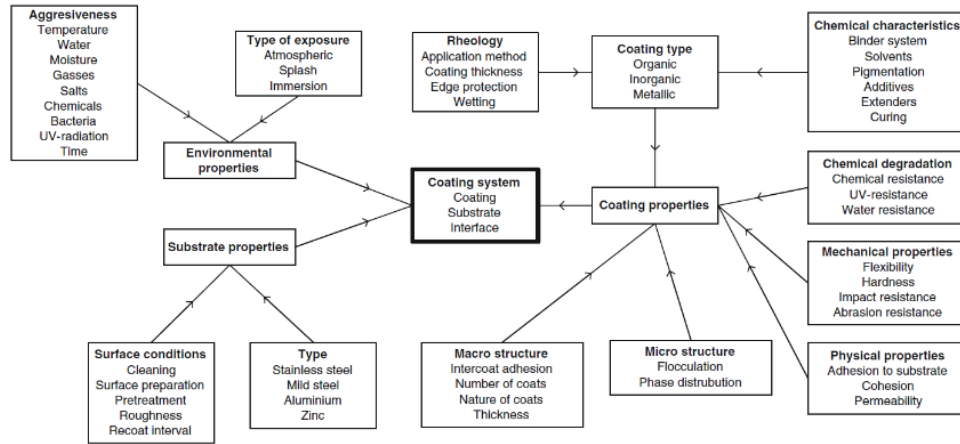
Figure III. Factors that affect the durability of an anti-corrosive coating.[3]

The next way of controlling corrosion is the selection of the appropriate polymer binder. Epoxies, acrylics, polyurethanes, silicones, and chlorinated rubber are all appropriate materials for anti-corrosive coatings. Epoxy systems are known for their excellent mechanical properties, good adhesion to metal substrates, and superior chemical resistance. However, epoxies are susceptible to UV photodegradation, which results in loss of performance properties. Acrylics have excellent UV stability and mechanical properties. Polyurethanes have superior water resistance and good abrasion resistance. Silicones have high flexibility, chemical resistance, and temperature stability. Finally, chlorinated rubber has very good water and vapor barrier properties, excellent adhesion, but low solvent resistance.

Coating systems provide corrosion control through a variety of pathways including creating an effective barrier against water and oxygen, creating a path of high resistance that inhibits anode-cathode interactions, passivating the metal with soluble ions, and providing another anode for dissolution of ions.[2] Along with polymeric coatings, anti-corrosive pigments are employed to prevent corrosion to limit anode-cathode interactions. There
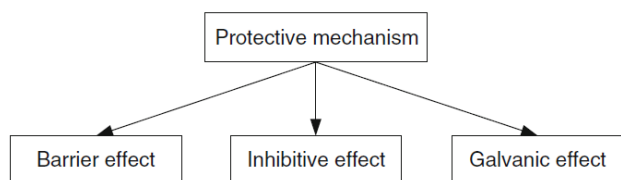
Figure IV. Protective mechanisms of anticorrosive coatings.[3]

3

are three types of corrosion pigments: inhibitive, galvanic, and barrier (**Figure IV**).[3] Inhibitive

pigments are chemically-active and release soluble species into any water that migrates in the

coating. The activated species are carried to the substrate, produce a protective or passivating

layer to inhibit corrosion. These inhibitive coatings are usually incorporated within the primer

layer in order to provide a shorter path to the metal substrate.[3] The effect of the inhibitive

coating is more notable when the diffusion of water into the coating necessitates the barrier

properties of the polymer coating. Some common pigments used are zinc chromate, strontium

chromate, red lead, zinc phosphate, silicates, and molybdates. Another type of anti-corrosive

pigments is galvanic, where the pigments act as an anode of a corrosion cell and will corrode

more rapidly than the substrate. Again, these systems are applied only as primers because the

pigment requires direct contact with the substrate and high loading of material is required for

good contact and electron flow.[3] Zinc metal powder is a common sacrificial pigment used due to

its high electrical activity and will corrode faster than the substrate. Barrier pigments are the

final type of anti-corrosive pigments. These materials are always inert, and are flake or plate-

like in shape to slow down the ingress of corrosive species in the coating. The protection of the

barrier pigment is highly dependent on the thickness of the applied coating, where delamination

of the coating decreases as film thickness increases.[3] Titanium dioxide, micaceous iron oxide,

and mica are all common barrier pigments incorporated into coating systems to provide a more

tortuous path for water and oxygen that migrate into the coating. Knowledge of anodic initiation

of corrosion on steel is still not widely understood and cannot subsequently be prevented or

detected. The employment of fluorescent probes to understand this anodic corrosion will allow

for the detection and prevention of corrosion.

1.3 Quantifying and understanding coatings during early corrosion detection

The inherent problem with the aforementioned systems is they only provide visual corrosion detection, which is highly subjective, extremely difficult to quantify, and limited to surface inspection.[4] Research is now directed to responsive and sensitive polymers for corrosion detection within seconds of exposure to corrosive elements (i.e. air, water, and electrolytes). Polymer coatings that respond to internal/external stimuli in addition to serving protecting and aesthetic roles are known as "smart coatings".[5] Some examples include self-healing films and the use of inhibitors that are released *in situ* when corrosion occurs.[5] However, one approach that has not been adequately addressed is the ability for the coating to detect and report the early effects of corrosion before any major damage has occurred. Quantifying these early initiation events would prevent further material damage while the damage costs are relatively inexpensive. A "smart" coating system that would detect early metal corrosion by tethered and free small molecule indicator probes that fluoresce in the presence of ions produced during the corrosion process could provide a solution to this problem. The fluorescence could be non-destructively measured, which could allow for necessary maintenance to be performed.[5] In one instance, the "turn-on" mechanism of fluorescence can proceed by two paths, with the first being the opening of a spirolactam ring by transfer of a proton into the system.[6, 9] The stability of this type of probe is limited by reactivity of reactants as well as the pH of the solution. In order to combat
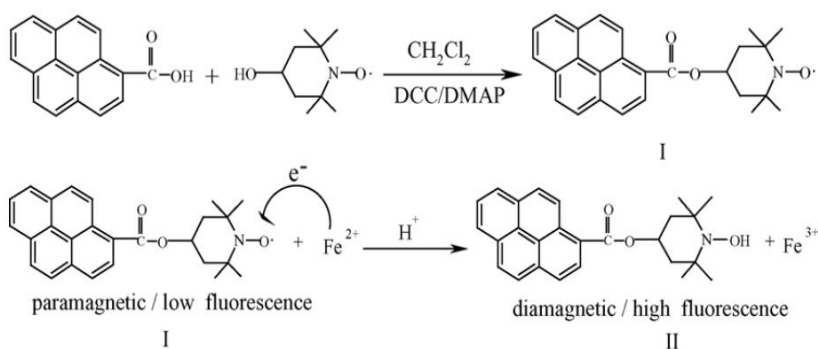
Figure V. Synthesis of pyrene-TEMPO fluorescent probe.[7]

this issue of stability, a probe with pH stability as well as stability in the presence of reactive

species in the solution is required to achieve the best fluorescence response. In the present study, a pyrene-TEMPO spin-label fluorescent probe has been proposed to address this problem. The probe proposed in Chen et al.[7] is a highly selective probe for iron II ion detection by a redox reaction between iron II and the pyrene-TEMPO probe.[7] The literature-based synthesis procedure of the pyrene-TEMPO spin label is presented in **Figure V**.

The goal of the research was to determine the fluorescent responsiveness of the pyrene-TEMPO probe in iron II rich environments. Fluorescent measurements were taken with a fluorimeter on solutions containing iron II and the probe at an excitation wavelength of 250 nm.[7] As the concentration of the iron II solution was increased from 0 to 3.6 (10^{-6} mol/L), a three-fold increase in fluorescence intensity at 430 nm was observed.[7] Also, weak fluorescence was observed in acidic solutions, which means that this probe was not easily affected by the protons produced at low pH values. The data also demonstrated a high selectivity for only the iron II ion, which permitted greater discernment and potential detection limits. While the results of this experiment are extremely important, these are not sufficient to qualify and quantify the probe characteristics blended and trapped within a glassy polymer film. In our research, we wanted to better understand the behavior of the probe in a polymer system in order to more clearly comprehend the mechanism of corrosion on coated steel substrates. We were not able to find any definitive research in the open literature regarding the protocols for probe loading or efficacy of probes within varying viscosity and physical states. .

2. Purpose of Research

Corrosion costs hundreds of billions of dollars each year in replacement and maintenance of infrastructures such as bridges and skyscrapers. To provide some relief to these costs and reduction in material loss, protective polymeric coatings and anti-corrosive pigments are

employed to hinder and prevent the corrosion process from occurring. Currently, corrosion detection process is extremely limited, and most methods rely on visual detection which is highly subjective and imprecise. A better understanding of the initiation and mechanisms of corrosion utilizes metal chelating probes to provide early visual or UV detection of the process. While these metal chelating probes provide accurate detection of the corrosion process, the information regarding the correct implementation and loading for coatings systems is unknown. Literature supports that a pyrene/TEMPO moiety will chelate to the iron II ions produced during the corrosion process and this provided the motivation for the use of this probe of our research. The goal of this research was to synthesize and employ polymer-tethered and free iron II ion sensing fluorescent probes to several model polymeric matrix materials and investigate the responsiveness when exposed to corrosive species. Starting and "turn-on" fluorescent efficiency were compared for the tethered and free probes to determine the optimal use and loading protocol.

In the polymer-tethered state, the probe is not able to freely diffuse and combine with the ions produced in the corrosion process. For this reason, we hypothesize that if the probe is covalently attached to the polymer resin, then fluorescence intensity will decrease due to the lack of diffusion of the probe, which leads to a decrease in collision frequency between the probe and its target ions. We further hypothesize that leaching of the probe will decrease as a result of covalent attachment to the polymer chain because of restricted mobility of the probe. The proposed research is composed of three main tasks:

1. Solution studies for probe response in the presence of iron species and pH changes for concentration determination.

2. Incorporation of probe into thermoplastic resins to attempt to understand the response changes in solvated and dried resins.

3. Leachate and corrosion studies between probes, corrosion detection, and thermoplastic resin.

The proposed research was expected to provide a better understanding of corrosion initiation at anodic sites, which is useful for the advancement of our understanding of anodic corrosion initiation and contribution to the broader impact of prevention of corrosion on steel substrates.

3. Research Objectives and Methodology

Research Objective 1: The first objective was to observe the fluorescence detection and discernment efficiency of metal ion chelators (i.e. iron (II)) in untethered solution systems. The first task was to perform solvent/aqueous solution studies to determine the appropriate probe concentration to achieve the desired fluorescence response without the resin. These tasks were designed to determine experimentally the concentrations of the probe necessary to achieve observable fluorescence values in specific utilized solvents and aqueous solutions, with the initial values coming from previous literature studies.[7,11,13] Once the values were determined, evaluation comparing conditions and concentrations of iron (II) sulfate solution required to achieve observable fluorescence values were determined. Calibration curves of concentration versus fluorescence response were produced to allow direct correlation of the intensity back to approximate concentrations to be made when the response in the polymer film was measured. The final step for this objective was to calculate the concentrations of phenoxy resin and solvent required to achieve observable fluorescence values in order to establish the limits of detection at both extremes.

Research Objective 2: Once the solution studies were complete, the probes were freely blended into available thermoplastic phenoxy resins for corrosion detection. Some of the available resins include materials in the PK (phenoxy) series: PKHA, PKHB, PKHB+, PKHH, PKHJ, and PKFE, which differ only in molecular weights that range from twenty-five thousand to sixty thousand, and T_g values that range from 80°C to 98°C. Some items that were investigated were the amount of polymer solution needed to cast films of desired thicknesses, percent solids (probe and resin), and viscosity of the material. The first step was to combine the probes with chosen resin system, then experimentally evaluate the concentrations of probe necessary to achieve observable fluorescence values. A peak intensity will be chosen as to ensure not to max out the instrument in the presence of iron (II) from the previous objective. The concentration of iron (II) chloride needed to achieve observable fluorescence values will be experimentally evaluated and compare the response to the calibration curve created from the solution studies. Once the values were established for the probe, varied scaled concentrations of resin and solvent were produced to achieve observable fluorescence values after application.

Research Objective 3: The final objective involved further leachate studies of the incorporated probes to polymer films, where the observed changes in the fluorescence data between the solution state and the applied film by *in situ* response to chloride anion (from the iron (II) chloride solution). Studies of the fluorescence changes in the system from the solution state to cast film were quantified during the casting, annealing and/or ageing processes to understand the longevity of the film and probes. We quantified any changes in fluorescence efficiency from the applied film to the dry coating. During this process, the effectiveness of the tethered probe was evaluated regarding the corrosion detection limits in the dry coating of both the tethered and untethered systems. Coupled with the fluorescence data, corrosion studies for early detection in

accelerated weather chambers was included to understand the longevity and detection methods of these probes in different environments.

4. Experimental

4.1 Materials

All chemicals were used as received and had no further purification methods unless otherwise stated. 1-Pyrenecarboxylic acid (Pyr.) was purchased from Tokyo Chemical Industry (TCI) dichlorobenzene (DCB), and 4-(dimethylamino)pyridine (DMAP) were purchased from Aldrich. Dicyclohexylcarbodiimide (DCC), 4-hydroxy-2,2,6,6-tetramethylpiperidine (TEMPO), and cyclohexanone were purchased from Acros Organics. Dichloromethane (DCM), chloroform (CHCl$_3$), methyl ethyl ketone (MEK) were purchased from Fisher. Ethyl 3-ethoxypropionate (EEP) was purchased from Eastman Chemical. Thermoplastic poly(hydroxyether) (Phenoxy®) resins were purchased form Gabriel Performance Products. These resins are linear thermoplastic diglycidlethers of bisphenol A (DGEBA) that have been ring opened to form hydroxyethers that contain secondary hydroxyls in place of the epoxide rings (**Figure VI**). The chosen resin was PKHH (52, 000 g mol^{-1}, T$_g$ = 86°C (DSC)).
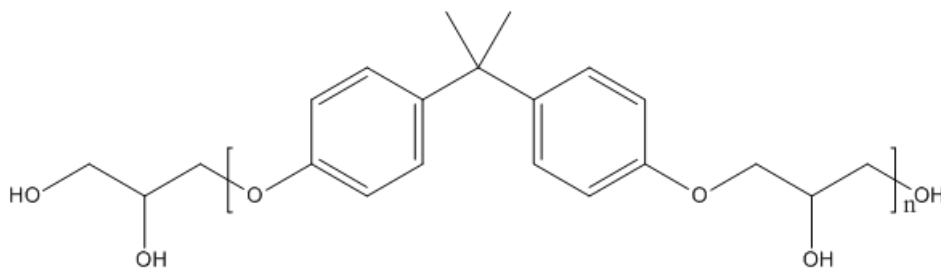
Figure VI. Primary structure of Phenoxy® poly(hydroxyether).

Thin layer chromatography (TLC) plates were purchased form Selecto Scientific. The 0.5 mL glass flat bottom vials were purchased from Laboratory Supply Distributors, Corp. Metal

substrates used were SAE 1008/1010 mild steel supplied by Q Panel with a "Type R" finish (dull matte mill finish of 25-26 µ inches). Substrates were polished with acetone to remove the oxidized zinc from the surface.

4.2 Synthesis of pyrene-1-(carboxylic)-(4-(2,2', 6,6'-tetramethyl- piperidine-N-oxide)hydroxy (pyrene-TEMPO).

The synthesis procedure of pyrene-TEMPO was adapted from recent literature sources.[7, 12, 13] An amount of Pyr. (0.5 mmol) [246.26 g mol^{-1}], TEMPO (2.0 mmol) [172.24 g mol^{-1}], and DMAP (0.305 mmol) [122.17 g mol^{-1}] were combined in a 40 mL amber vial with 20 mL of DCB and ACN at room temperature. The resulting mixture was brought to 0 °C, and DCC (0.55 mmol) [206.33 g mol^{-1}] was added dropwise to the mixture. After five minutes, the cooling bath was removed, and the mixture was allowed to warm up to room temperature and react overnight. The mixture turned from turn pale yellow to white due to the formation of dicyclohexyl-urea (DCU). The resulting product was centrifuged to remove the precipitate and any unreacted materials (3000 RCF for 3 min.). The product was washed with 20 mL 1-propanol/Deionized (DI) H_2O (1:1 v:v), and the organic (bottom) layer was collected. A dark orange solution was obtained, and the remaining solvent was removed in a vacuum oven overnight. The solid product was dissolved in a small amount of Hex:EtOAc (9:1 v:v). Product separation was achieved by column chromatography using SiO_2 as the stationary phase and Hex:IPA (9:1 v:v) as mobile phase. An amount of 1-propanol/DI H_2O (1:1 v:v) (200 mL) and the stationary phase were combined to achieve a slurry. The slurry was poured into the column and allowed to equilibrate overnight. The product dissolved in Hex:EtOAc (9:1 v:v) was loaded onto the column and run with Hex:EtOAc (9:1 v:v) as the mobile phase. Two distinct fractions were collected from the column. The solvent was removed from both fractions by roto-evaporation, and the resulting slurries were placed in a vacuum oven to remove additional solvent. TLC was

performed on flexible silica gel plates (200 µm) to confirm a single spot that was different than the starting materials. The plates were spotted with 2 µL of sample in each spot. Hex:EtOAc (9:1 v:v) was used as the mobile phase to achieve R_f (ratio between migration distance of a substance and the migration distance of the solvent front) values of 0.29 for the product compared to 0.12 for the pyrene and 0.02 TEMPO spots. A 2 mmol L^{-1} stock solution was prepared from the first fraction, with a solvent blend as the diluent (21.05 wt.% cyclohexanone, 26.3 wt.% EEP, and 52.65 wt.% MEK). A 2:1 serial dilution was prepared from this stock solution, and the results were reported in **Table I**.

4.3 Characterization of Aqueous Iron II/Pyrene-TEMPO Moiety

LC/MS

The synthesized pyrene-TEMPO (PT) probe was characterized by liquid chromatography-mass spectrometry (LC/MS; Varian) to determine M/Z values. Samples were prepared by a 4:1 dilution of 2 mM PT stock solution to achieve a final concentration of 0.2 mg/mL and a final volume of 1 mL.

Fluorescence

Fluorescence measurements were performed on a TECAN infinite M1000 Pro instrument. In aqueous studies, triplicate 300 µL samples were taken from each of the serial dilutions and were placed into 0.5 mL glass flat bottom vials (9x17 mm) in a polystyrene 96-well plate for analysis on the TECAN instrument. A 2 mM $FeSO_4$ stock solution was prepared and serial dilutions were performed to yield the concentrations listed in **Table II**. The 1µM PT dilution was the chosen concentration to be added to each of the iron II samples for the fluorescence studies. Absorbance spectra was gathered from 300-500 nm, with a bandwidth of 10 nm and a step size of 1 nm to determine the maximum excitation wavelength. According to Chen et. al.[7], the maximum excitation and emission values were 346/399 nm, respectively.

Using the excitation data, a fluorescence sweep was taken from 320-480 nm, with a bandwidth of 5 nm and a step size of 1 nm to determine the maximum emission value.

^{1}H NMR

Samples were prepared for NMR analysis with a concentration of 10 mg/mL in CDCl$_3$. Acquisitions were done with 32 scans with 5 sec delay times between scans on a Bruker 300 MHz NMR Spectrometer. All data was baseline and phase corrected in MestReNova software.

ATR-FTIR

A Nicolet^{TM} 6700 FTIR (Thermo Scientific) equipped with a SMART iTR attachment was used to analyze the product in the 4000 - 650 cm^{-1} range and operated in ATR mode at a resolution of 2 cm^{-1} and 32 scans per sample.

Accelerated Weather Chambers

The scribed and non-scribed coated steel panels were evaluated as per ASTM B117 and GM 14872 with the exposure area defined by taping the panel edges with 3M 8992 polyester film tape.[14-15] ASTM B117 maintained a fog of 5% NaCl solution and a constant cabinet temperature of 35 °C. GM 14872 cycles through three steps:

1) three minutes spray of a blend of 0.9 wt% NaCl, 0.1 wt% CaCl$_2$, and 0.0075 wt% NaHCO$_3$, temperature of 25 °C, and 45 % relative humidity (RH) maintained for eight hours

2) one-hour ramp to 49 °C and 100% RH maintained for eight hours

3) three hours ramp to a dry stage at 60 °C and 25% RH maintained for eight hours.[14-15]

5. Results and Discussion

5.1 Aqueous Studies

The synthesis process was altered from the observed literature and several iterations were required to determine the proper solvents, molar quantities, and reaction conditions. Many of the synthesis procedures listed in the literature employed a pyrene butyric acid along with 4-amino-TEMPO to achieve faster reaction rates and better coupling efficiency as well as the robustness of the amide linkage. However, this butyl chain in the pyrene butyric acid unit would render the probe useless in observing a "turn-on" mechanism of fluorescence in iron solutions because it is not fluorescently active. However, the pyrenecarboxylic acid used in our synthesis has less mobility as well as more steric hinderance in the reaction, making it difficult to couple to 4-hydroxy-TEMPO through the Steglich Esterification reaction. The solvent selection was key in solubilizing and stabilizing all reactants to achieve maximum reactivity in the solution. Pyrene was particularly difficult to dissolve and caused issues in achieving the desired pyrene-TEMPO product. After five iterations (seven in total), a mix of DCB and ACN was employed as the solvent to achieve maximum solubility of the pyrene, while selectively precipitating the DCU from solution. A lower molar quantity of pyrene than was reported in the literature (0.5 mmol vs. 8.12 mmol) was required to achieve solubility of the pyrene in the chosen solvent system of 80:20 v:v DCB:ACN. After the reaction, a DI H_2O wash removed any remaining DCU as well as TEMPO and DMAP. Column chromatography was also employed to further separate and ensure the TEMPO and DMAP were removed from the final product, which was confirmed by LC/MS. There were three distinct spots on the TLC plates that corresponded with TEMPO, DMAP, and the PT product. The wash solvent for the silica gel column with 90:10 v:v EtOAc:Hex as the stationary phase was chosen based on the largest separation observed by TLC. The mobile phase was chosen from several different combinations of Hex:EtOAc (9:1, 1:9, 1:0)

in order to determine the optimal solution, which was 9:1. Once column chromatography was performed to further separate and purify the product, which yielded two distinct fractions, each of the fractions were roto-evaporated to yield a yellow/orange powder-like solid. NMR analysis was performed on each fraction for which the results are shown in **Figure VII** and **Figure VIII** below.
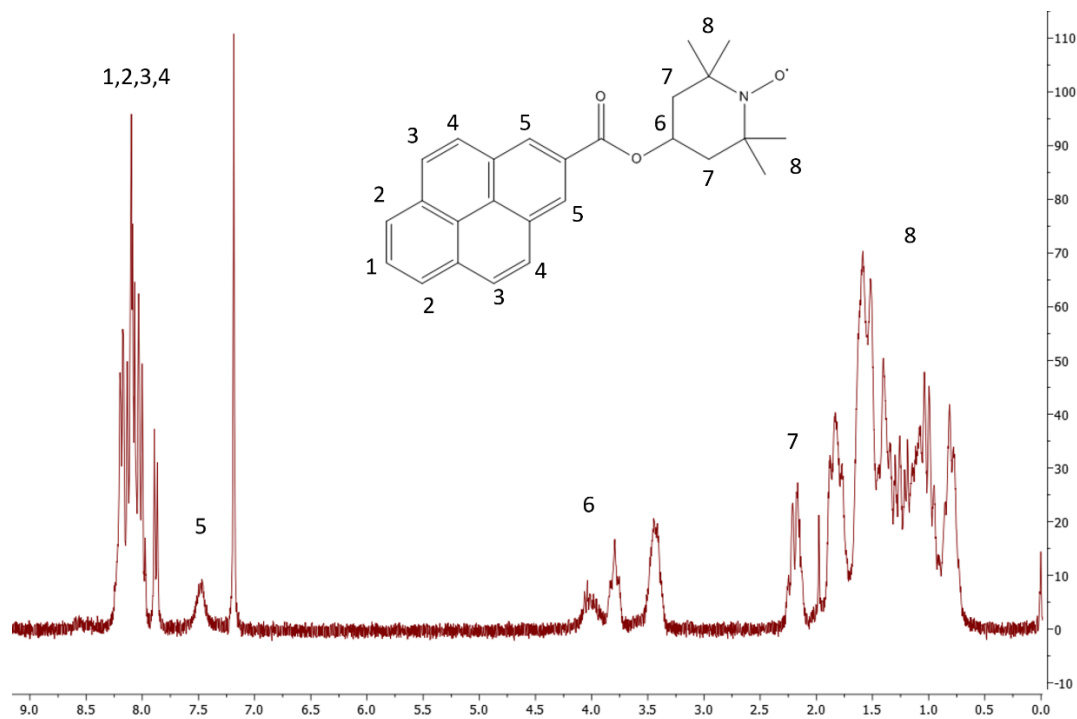
Figure VII. ^{1}H NMR analysis of PT Fraction 1 in CDCl$_3$.

15
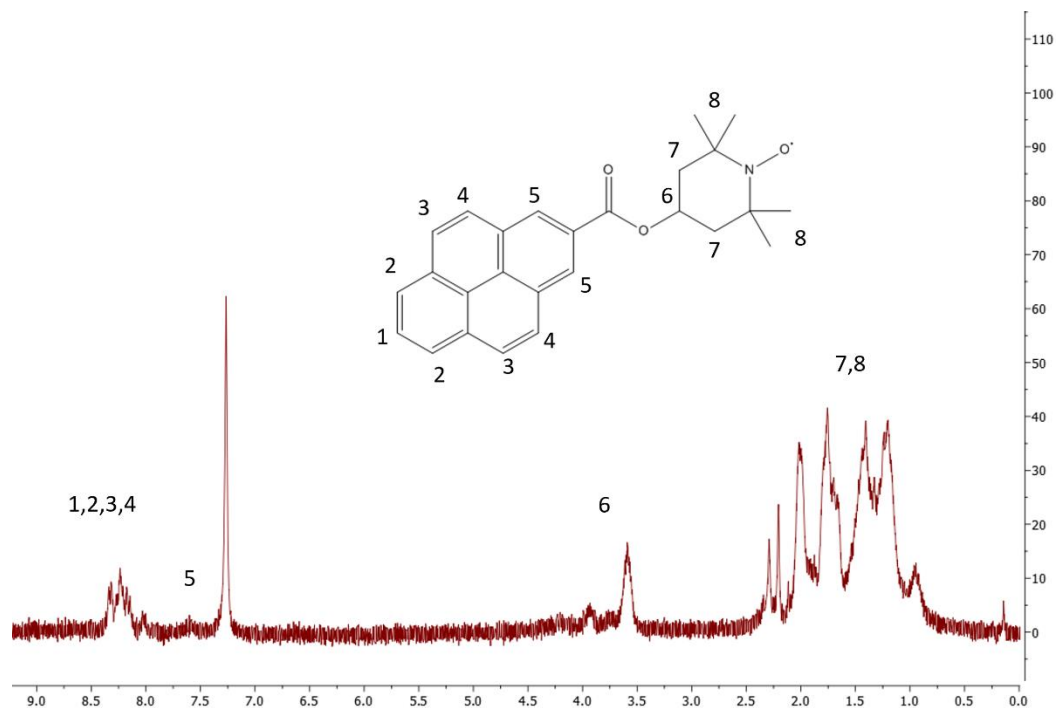
Figure VIII. ^{1}H NMR analysis of PT Fraction 2 in CDCl$_3$.

Integration of the peaks located from 7.5 to 8.8 ppm (corresponding to the aromatic protons) in

Figure VII indicate that they are about two times less than that of the peaks located from 0.8 to 2

ppm (corresponding to the TEMPO protons). These two spots correlate to the 9 protons of the

pyrene section of the probe and the 17 protons of the TEMPO section respectively. We do not

observe the same trend in integration for fraction 2 in **Figure VIII** due to the large amount of

unreacted TEMPO present, since it was used in four times excess. TLC also confirmed that

fraction 2 contained a large amount of unreacted TEMPO as well as some DMAP, while fraction

1 yielded only one spot on TLC when run in 9:1 Hex:EtOAc v:v, which indicated that it

contained no observable impurities. Once the product was confirmed by TLC, a serial dilution

was performed to yield the values below in **Table I**.

Table I. 2:1 Serial Dilution of PT in ACN to achieve concentrations ranging from 10 to 0.0625 µM.

| Probe Concentration (µM)	10	1	0.5	0.25	0.125	0.0625
Transfer Volume (µL)	10	200	1000	1000	1000	1000
Diluent Volume (µL)	1990	1800	1000	1000	1000	1000
Total Volume (µL)	2000	2000	2000	2000	2000	2000

A similar serial dilution was performed in $FeCl_2$ that was used in fluorescent studies to understand the shift or intensity changes in fluorescence when complexed. A 2mM stock solution was made with $FeCl_2$ in ACN (**Table II).** Once the two dilutions were prepared, they were combined (keeping the concentration of $FeCl_2$ constant in each solution) in order to yield **Figure IX** and **Figure X**, which represent 1 µM solutions of both PT and Fe.

Table II. 2:1 Serial Dilution of $FeCl_2$ in CAN to achieve concentrations ranging from 10 to 0.0625 µM.

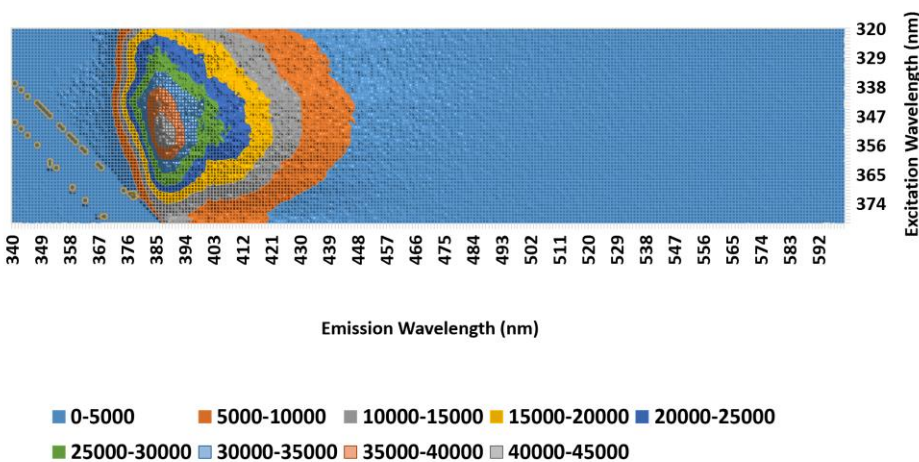| $FeCl_2$ Concentration (µM)	10	1	0.5	0.25	0.125	0.0625
Transfer Volume (µL)	10	200	1000	1000	1000	1000
Diluent Volume (µL)	1990	1800	1000	1000	1000	1000
Total Volume (µL)	2000	2000	2000	2000	2000	2000

PT F1 iron dose response
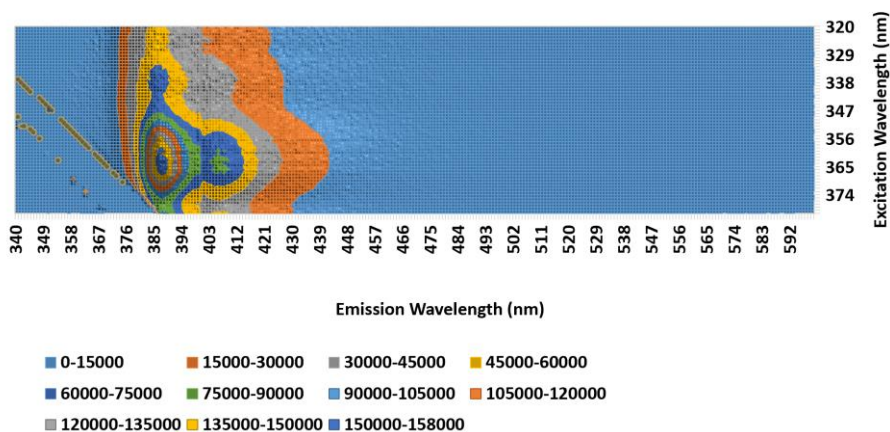
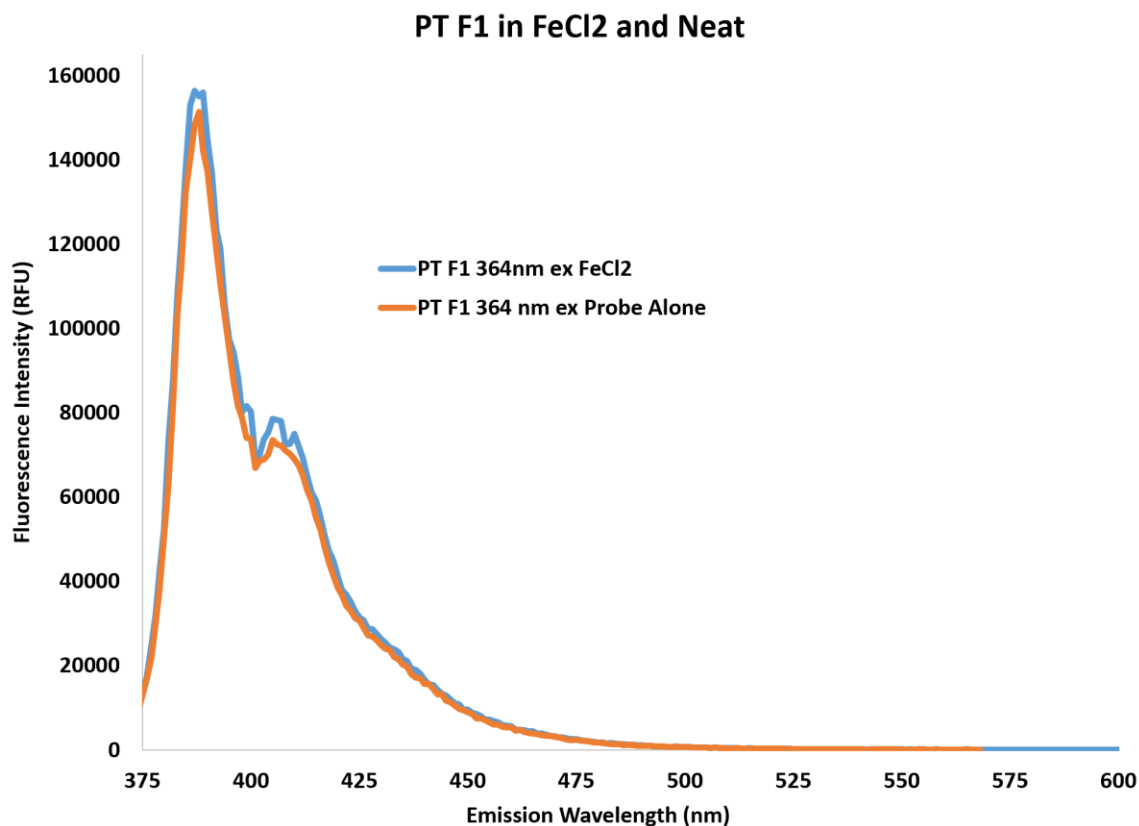**Figure IX.** 3D fluorescence intensity scan on PT F1 sample at 1 µM in ACN to yield excitation vs. emission plot.

PT F2 iron dose response

Figure X. 3D fluorescence intensity scan on PT F2 sample at 1 µM in ACN to yield excitation vs. emission plot.

Figures IX and **X** display 3D fluorescence intensity scans representing the maximum excitation and emission values. From the figures above, the highest intensity for both fractions was observed at an emission wavelength of 387 nm, which was about 10 nm blue shifted from the literature.[7] For fraction 1, 387 nm emission wavelength corresponded to a 364 nm excitation wavelength, while fraction 2 was different with an excitation wavelength of 354 nm (slightly

18

red-shifted). The intensity of fraction 2 at 387 nm emission wavelength was almost 4 times less than fraction 1. Fraction 1 also exhibited a slight shoulder at 435 nm emission wavelength that was like the observed shoulder in literature[7]; however, the shoulder was non-existent in the fluorescence spectra of fraction 2. Intensity vs. emission wavelength was plotted for fraction 1 without $FeCl_2$ and with $FeCl_2$, and the results are shown in **Figure XI**.

Figure XI. PT Fraction 1 in iron and Probe alone plotted at 364 nm excitation wavelength to yield a graph of fluorescence intensity vs. emission wavelength.

PT F1 iron and acid dose response
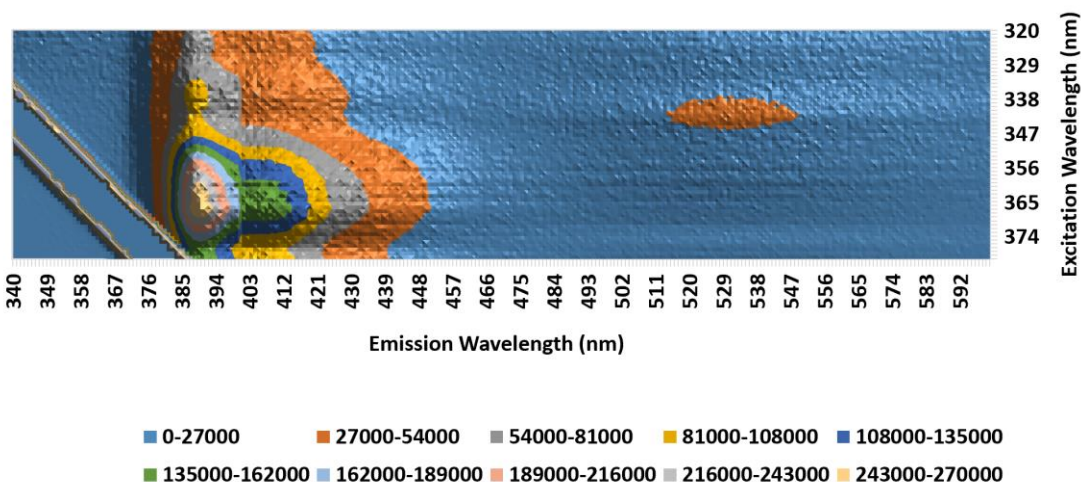
Figure XII. 3D fluorescence intensity scan on PT F1 sample at 1 µM in iron II and sulfuric acid in ACN to yield excitation vs. emission plot.

When comparing fraction 1 in the probe alone and iron dosed samples, there is a 4000-fluorescence intensity increase upon addition of $FeCl_2$ into the systems due to the "turn-on" mechanism of the probe. Since the "turn on" mechanism proceeds by the donation of an election from Fe^{2+} species in the solution, we understand that the mobility of the free probe in solution allows for the highest observable fluorescence intensity as opposed to the resin or glassy polymer state. The latter two states would possess much less free mobility, therefore decreasing the collision frequency of the probe and iron. The fluorescence figures give us an accurate representation of the behavior of the probe in solution as well as good indications to the location and relative intensity scales that would be expected for the other two states. Upon addition of 10 µL of 6 M H_2SO_4, the relative fluorescence intensity of the PT fraction 1 solution doubled due to the enhancement of the probe in acidic aqueous media. **Figure XIII** contains the plot of PT

20

fraction 1 in $FeCl_2$, and Probe alone, and in $FeCl_2 + H_2SO_4$, at the maximum excitation
wavelengths.
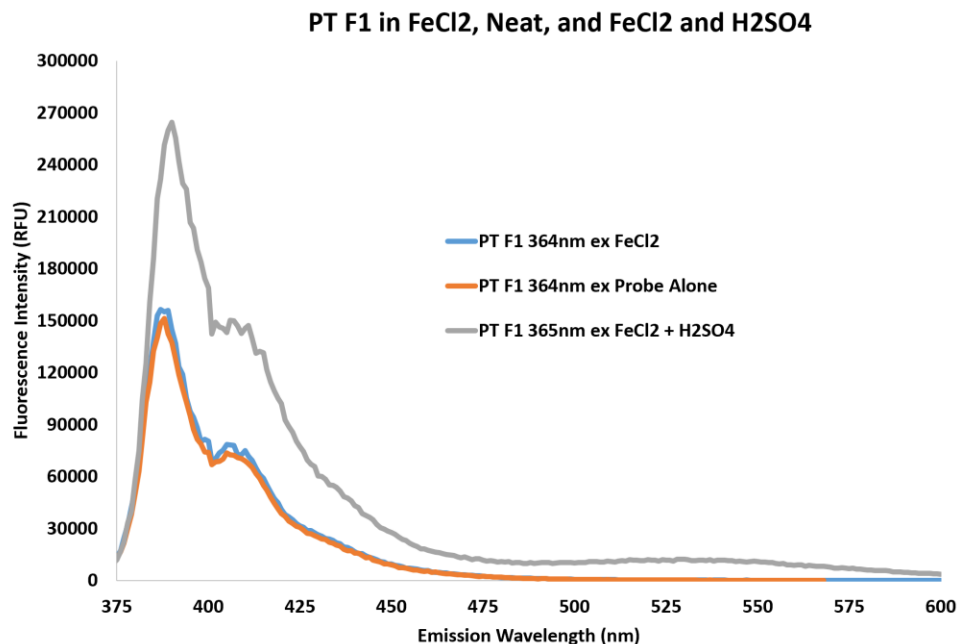
Figure XIII. PT Fraction 1 in $FeCl_2$ and Probe alone and in $FeCl_2 + H_2SO_4$ at 364 and 365 nm excitation
wavelength.

The increase in intensity was promising for the implementation of this probe into coatings on
steel substrates because the operating pH around a point of failure where Fe^{2+} is being generated
as a result of pitting corrosion is about 4. This means that at the pH decreases, we would observe
an enhancement of fluorescence signal.

6. Conclusion

Significant work is still required in order to fully quantify and observe the corrosion process
in a fast and efficient way. Modern coatings scientists still rely upon visual inspection of coated
metal substrates to determine corrosion initiation, growth, and failure points, and this process
requires higher amounts of money to be spent in repair and maintenance. Coatings with early
detection and embedded monitoring thereof provide new quantifiable ways to detect mechanistic

processes and dependencies and are capable of aiding, monitoring, and preventing corrosion from occurring with improved timing for maintenance and repair of coated substrates. The use of fluorescent probes is one avenue of detection being investigated in recent studies. The probe of choice in our study was a pyrene-TEMPO moiety capable of selective detection of Fe^{2+} in acidic aqueous media. The synthesis of this probe proved to be difficult to repeat from the cited literature due to limited descriptions of key synthetic procedures, so the majority of this work involved seeking and designing a synthesis route that would provide ease of reproducibility as well as advance the knowledge of the characterization of the probe itself. As shown by the results displayed in **Figures VII-XIII**, we were able to successfully synthesize the desired probe through the application of DCB:ACN as the solvent and the molar and synthetic conditions listed above. We were also able to determine the accuracy of this probe based on its fluorescence in iron rich-environments as well as acid-rich environments. The fluorescence of the probe was enhanced two-fold in acidic/iron environments, which allowed for better understanding of the "turn-on" mechanism.

Future Work

Research objectives 2 and 3 were not able to be met in the time frame of the thesis project; however, they play a major role in the usefulness of this probe as a means of corrosion detection. Significant work needs to be completed to achieve the maximum benefit of the probe synthesis and the data that can be collected from its incorporation into polymer coatings. Since the mobility of the probe will be restricted in a resinous system as well as a glassy polymer coating, the intensity and emission wavelengths will most likely be hindered and shifted from the data collected in the aqueous state. The low pH is required to achieve an increase in fluorescence

22

intensity, the pH of the coating needs to be predetermined and monitored to distinguish between

the coating chemistry and the corrosion process, especially for the initiation moments.

7. References

1. Davis, J.R. *Corrosion: Understanding the Basics*; Davis & Associates: Materials Park, Ohio, 2000.

2. Forsgren, Amy. *Corrosion Control Through Organic Coatings*; Philip A. Schweitzer, P.E.: York, Pennsylvania, 2006. pp.1-26.

3. Sørensen, P.A. Anticorrosive Coatings: A Review. *J. Coat. Technol. Res.* **2009**, 6, 135-176.

4. *The North American Technology and Industrial Base Organization*. Corrosion Detection Technologies: Sector Study. BDM Federal, Inc., 1998.

5. Augustyniak, A., Tsavalas, J. and Ming, W. Smart Epoxy Coatings for Early Detection of Corrosion in Steel and Aluminum. *Prog. Org. Coat*. **2011**, 71, 406-412.

6. Augustyniak, A., Tsavalas, J. and Ming, W. Early Detection of Steel Corrosion via "Turn-On" Fluorescence in Smart Epoxy Coatings. *ACS Appl. Mater. Interfaces*. **2009**, 1 (11), 2618-2623.

7. Chen, J.L. High selective determination iron(II) by its enhancement effect on the fluorescence of pyrene-tetramethylpiperidinyl (TEMPO) as a spin fluorescence probe. *Spectrochimica Acta Part A*. **2005**, 63, 438-443.

9. Venancio, P., Cottis, R., Narayanaswamy, R. Optical sensors for corrosion detection in airframes. *Sensors and Actuators B: Chemical*. **2013**. Vol. 182. 774-781.

10. Wu, J., Liu, M., Zhuang, X. Fluorescence Turn on of Coumarin Derivatives by Metal Cations: A New Signaling Mechanism Based on C=N Isomerization. *American Chemical Society*. **2006**.

11. Hirayama, T., Okuda, K., Nagasawa, H. A highly selective turn-on fluorescent probe for iron(ii) to visualize labile iron in living cells. *Chemical Science*. **2013**. Vol. 4 (3). 1250.

12. Dang, S., Ma, E., Sun, Z. A layer-structured Eu-MOF as a highly selective fluorescent probe for Fe3+ detection through a cation-exchange approach. *Journal of Materials Chemistry*. **2012**. Vol. 22 (33). 16920.

13. Ottaviani, M., Venturi, F., Pokhrel, M. Physicochemical Studies on the Adsorption Properties of Asbestos 2. An EPR and Fluorescence Study on the Adsorption of Pyrene. *Journal of Colloid and Interface Science*. **2001**. Vol. 238. 371-380.

14. ASTM B117-18, *Standard Practice for Operating Salt Spray (Fog) Apparatus*, ASTM International: West Conshohocken, PA, **2018**.

15. GMW14872, *Cyclic Corrosion Laboratory Test*, General Motors Worldwide **2018**.